Analysis of the Mechanical Behavior of a 20T Hybrid Cos Dipole During Quench Transients

Analysis of the Mechanical Behavior of a 20 T Hybrid Cosθ Dipole during Quench Transients

Marika D'Addazio, Paolo Ferracin, *Senior Member, IEEE*, Emmanuele Ravaioli, Laura Savoldi, *Senior Member, IEEE*, Giorgio Vallone

***Abstract*—The US Magnet Development Program is conducting research on high-field accelerator magnets targeting a bore field of 20 T for the next generation of particle colliders. To reduce the overall cost of the dipole, a viable option consists in a hybrid approach where the inner coils in the high-field region are made of High Temperature Superconductors (HTS), such as Bi-2212 or REBCO coated conductors, and the coils in the lower field region (<16 T) are made of Low Temperature Superconductors (LTS), i.e. Nb_3Sn. Quench protection for high-field magnets is demanding, especially in the case of a full-scale 15 m long magnet. To mitigate these challenges, an innovative quench protection method named Energy Shift with Coupling (ESC) has been selected and integrated into the magnet design. This method requires resistive coils that are strongly magnetically coupled to the magnet coils and electrically insulated from them. In this contribution, a 20 T hybrid cos-theta dipole configuration is analyzed, investigating the stresses on the conductors during quench transients while limiting the adiabatic hot-spot temperature.**

***Index Terms*—Superconducting magnets, dipole, hybrid magnets, HTS, Nb_3Sn, quench protection, ESC, mechanical analysis.**

I. Introduction

THE U.S. Magnet Development Program (MPD) is leading a design study group focused on advancing accelerator magnet technology to support the next generation of high-energy physics colliders, as outlined in the program roadmap for 2025–2030 [1]–[3].

The practical limit of 16 T for the Nb_3Sn accelerator magnets does not allow to rely only on Low Temperature Superconductors (LTS) for achieving a target field of 20 T. A possible solution consists in the introduction of a hybrid concept, in which High Temperature Superconductors (HTS) are employed in the high-field region of the coils, while LTS conductors are used in the lower field region. This hybrid approach can also help contain the overall cost of the magnet, given that Nb_3Sn is currently less expensive and better mastered than HTS [4].

For magnets built with LTS conductors, different quench protection options have been explored and tested to prevent mechanical damage from quench events. For example, in [5] the authors present a 2D mechanical analysis of MQXF magnets protected with quench heaters, while in [6] are reported the results on the evaluation of the thermo-mechanical stresses during a quench transient in the Test Facility Dipole (TFD), a large aperture magnet under development at LBNL, where the quench protection relies on energy extraction.

The protection of such a high field hybrid magnet from the consequences of a quench presents significant technical challenges. The performance of a quench protection system based on Coupling-Loss Induced Quench (CLIQ) method [7], [8] has already been investigated in [9]. The results indicate that, for the current baseline of the Bi-2212/Nb_3Sn hybrid magnet design, one CLIQ unit charged to 1 kV can protect 1 m long versions of the magnet. In this configuration, the hot-spot temperature remains below 270 K and the simulated peak voltage to ground is 537 V. This protection method is sufficient to protect a magnetic length up to 5 m while keeping the adiabatic hot-spot temperature below 350 K. The protection of a full-scale 15 m long magnet adds further complexity and requires the investigation of innovative quench protection systems, such as the Energy Shift with Coupling (ESC) method [10], which was successfully demonstrated on a Nb_3Sn racetrack coil [11].

This manuscript presents the analysis of the 2D cross-section design of a 20 T hybrid cosθ dipole magnet integrated with ESC protection system, focusing on the challenges of managing mechanical stresses during a quench transient. The protection system requires resistive coils, electrically insulated from the magnet coils and magnetically coupled to them. A mechanical study, carried out under the assumption of an infinitely rigid structure, is performed to assess the feasibility of this innovative quench protection method for such a high-field magnet. Future analyses are planned with a real support structure to assess the stresses during quench transients. It is expected that the deformability of the structure will improve the stresses during transients, but may lead to worse results during energization, as discussed in [12]. The novelty of this work lies in demonstrating a viable approach to protecting a demanding magnet design that satisfies stress requirements, while also identifying potential critical points.

Automatically generated dates of receipt and acceptance will be placed here.

This work is part of the project PNRR-NGEU which has received funding from the MUR – DM 118/2023.

This work is supported by the Office of High Energy and Nuclear Physics, U. S. Department of Energy, under contract No. DE-AC02-05CH11231.

This work is partially supported by the High Field Magnet (HFM) program.

M. D'Addazio is with Politecnico di Torino, 10129 Torino (TO), Italy and Lawrence Berkeley National Laboratory, Berkeley, CA 94720 USA (e-mail: marika.daddazio@polito.it).

P. Ferracin and G. Vallone are with Lawrence Berkeley National Laboratory, Berkeley, CA 94720 USA.

E. Ravaioli is with the European Organization for Nuclear Research (CERN), 1211 Geneva, Switzerland.

L. Savoldi is with Politecnico di Torino, 10129 Torino (TO), Italy and Istituto Nazionale di Fisica Nucleare, sez. Genova, Italy.

Colour versions of one or more of the figures in this paper are available online at xx.

Digital Object Identifier: xx.

This article has been accepted for publication in IEEE Transactions on Applied Superconductivity. This is the author's version which has not been fully edited and content may change prior to final publication. Citation information: DOI 10.1109/TASC.2026.3666509

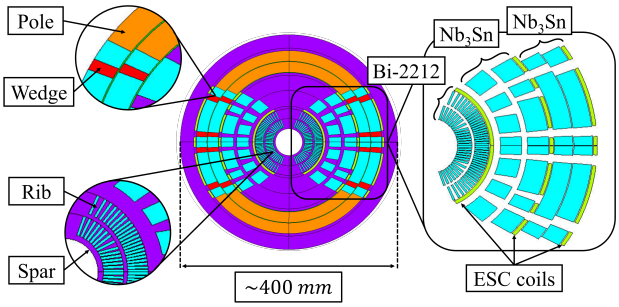

Fig. 1. A 2D cross-section of the dipole magnet, showing an overall diameter of 400 mm, including the stainless steel collar. On the right, a magnified view shows the superconductor layers made of Bi-2212 and Nb_3Sn and the copper ESC coils. On the left, the mandrel components (spar and ribs) and the traditional cosθ design elements (pole and wedge) are highlighted.

II. Magnet Design

A. 2D cross-section description

In this contribution, a 20 T hybrid cosθ dipole magnet is designed to reach a magnetic field of 20 T in a 50 mm clear bore aperture at a nominal current I_{op} of 11.6 kA and at a temperature of 1.9 K [2], [12], [13]. The load-line margin, defined as $(I_{ss} - I_{op})/I_{op}$, with I_{ss} the short sample current, is approximately 20% for all coils. The 2D cross-section of the magnet, including the stainless steel collar, is shown in Fig. 1. The magnet has six layers made of superconductor cables and includes three 1-layers copper ESC coils per pole.

The conductors selected for the design are Bi-2212 (HTS) and Nb_3Sn (LTS) designed as Rutherford cables made of multi-filamentary strands. The main conductor parameters are summarized in Table I.

To intercept electromagnetic forces and mitigate the stresses on the conductors, a mandrel, made of spar and ribs for layers 1-4 as shown in Fig. 1, is used to provide radial and azimuthal mechanical support. Layers 5 and 6 are designed in the standard cosθ configuration made of titanium winding poles and aluminum–bronze wedges impregnated with coils. A detailed description of the magnet support structure configuration is provided in [12], [13].

The three ESC coils are made of copper, and share the same mandrel design concept to intercept Lorentz forces. The final diameter of the magnet cross-section, as shown in Fig. 1, is approximately 400 mm, which is 18 mm larger than the value reported in [12] to accommodate the ESC coils. The operational current I_{op} does not account for the increased spacing between the superconducting coils, which would require a 1% current increase to maintain the same bore field. This ensures consistency with previous protection studies on this magnet configuration.

B. Description of ESC protection system

The main concept behind the ESC method is to drive the magnet into a resistive state through transient losses, with the dominant contribution in this case being the Inter-Filament Coupling Loss (IFCL) [14]–[17]. Part of the magnet's stored energy is then extracted by transferring it to the normal-conducting ESC coils. Due to their location near the superconducting coils and their similar geometry, the ESC coils are strongly magnetically coupled to the magnet coils and also mutually coupled to each other. When a quench is detected and the ESC units are triggered, a voltage is applied across the ESC coils, changing their current. Because of the magnetic coupling, this induces a change in the magnet current. One of the main advantages of the ESC protection method is that it allows for a change in magnet current without imposing a high voltage across the magnet coil.

As shown in Fig. 1, each magnet pole contains identical ESC coils, arranged as ESC-up and ESC-down. The connection configuration is as follows: the ESC-up and ESC-down in layer A are powered by one 50 mF, 250 V unit; the ESC-up coils in layers B and C are powered by one 50 mF, 500 V unit; and the ESC-down coils in layers B and C are powered by one 50 mF, 500 V unit. Based on the specific connection scheme, the ESC coil arrangement will be referred to as ESC 1, ESC 2, and ESC 3, respectively.

The main parameters of the ESC coils, summarized in Table II, result from an iterative process intended to meet the requirements for the adiabatic hot spot temperature and the equivalent peak stress, as discussed in detail in Section IV. ESC 1 has 60 turns up and 60 turns down in a single block, ESC 2 has 60 turns divided into four coil blocks in layer B and 73 turns divided into three blocks in layer C, while ESC 3 has the same configuration as ESC 2. In the current design, the turns of ESC 1 are not separated by the ribs. For a future study, the aim is to investigate a design where the coil of ESC 1 follows the same configuration as the HTS in layer 2. The ESC coils, similar to the superconducting coils, are modeled as a homogenized material in the mechanical simulations.

Regarding the ESC coil material, the main options under consideration are oxygen-free coppers (C10100–C10700), selected to ensure both high conductivity and adequate mechan-

TABLE I
Main Conductor Parameters

Parameter	L1-L2	L3-L4	L5-L6
Superconductor/Stabilizer	Bi-2212/Ag	Nb_3Sn/Cu	Nb_3Sn/Cu
Number of strands (-)	32	50	50
Strand diameter (-)	0.90	0.80	0.70
[1]Ag/noAg or Cu/noCu (-)	4.00	0.90	2.00
Cable width (mm)	14.87	22.16	19.39
Cable average thickness (mm)	1.70	1.52	1.33
Insulation thickness (mm)	0.15	0.15	0.15
Number of turns per quadrant (-)	37	76	104
Operating current I_{op} (A)	11593	11593	11593
Current density J_e at I_{op} (A/mm^2)	569	461	602
Peak conductor field at I_{op} (T)	20.29	15.86	12.22

[1] Stabilizer/Non Stabilizer ratio in the strand cross-section.

TABLE II
Main ESC coil Parameters

Parameter	ESC 1	ESC 2	ESC 3
Self inductance at I_{nom} (mH/m)	7.27	14.2	14.2
Number of turns (-)	60+60	60+73	60+73
Insulated cross-section A_{ins} (mm^2)	1100	1220	1220
A_{ins} with respect to magnet coil (%)	3.6	4	4
Wire width (mm)	3.55	3.55	3.55
Wire average thickness (mm)	1	1	1
Insulation thickness (mm)	0.10	0.10	0.10

This article has been accepted for publication in IEEE Transactions on Applied Superconductivity. This is the author's version which has not been fully edited and content may change prior to final publication. Citation information: DOI 10.1109/TASC.2026.3666509

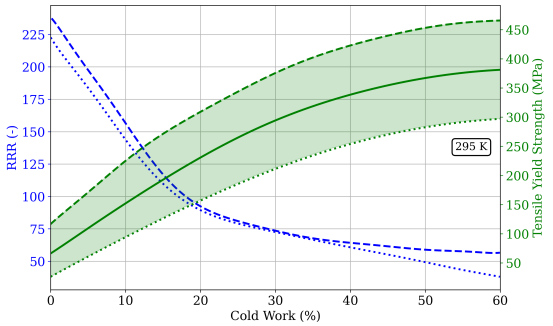

Fig. 2. Properties of oxygen-free copper: Residual Resistivity Ratio (RRR) and tensile yield strength as functions of cold work percentage [18].

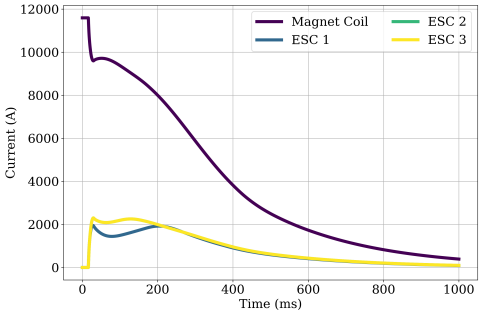

Fig. 3. Evolution of the current in the magnet and ESC coils versus time during a transient following the activation of the ESC protection system on 1 m long hybrid magnet.

ical strength at cryogenic temperatures. The main properties of copper at such temperatures are reported in [18], with the exception of the thermal expansion curve, which is obtained from [19]. To achieve sufficiently high tensile yield strength without significantly affecting the Residual Resistivity Ratio (RRR), the oxygen-free copper is specified to have approximately 30% cold work (CW). In Fig. 2, the RRR and the tensile yield strength (MPa) are shown as functions of the CW percentage, and these data were retrieved from [18]. A conservative yield strength value is adopted by reducing the nominal yield strength by 10% to account for uncertainties associated with the limited amount of data for copper in wire form. Under these assumptions, the tensile yield strength considered in the analysis is around 265 MPa, based on calculated values reported in [18], and the RRR value is 75.

III. Thermo-Mechanical Analysis During a Quench Transient

A. Modeling assumptions

The analysis of the stresses during a quench transient is carried out using results obtained from 2D electromagnetic-thermal simulations performed in STEAM-LEDET, which takes into account thermal diffusion in the coil windings, ohmic losses, and inter-filament coupling losses [20], [21]. In particular, the electromagnetic forces and temperatures computed in STEAM-LEDET are transferred, at selected time steps, to a 2D mechanical model in ANSYS APDL, following the same methodological approach described in [6]. In this study, the analysis assumes a magnetic length of 1 m, while the ESC protection system can protect the magnet for lengths up to 15 m.

The mechanical model assumes an infinitely rigid structure and simulates only magnet energization and quench transient. The mechanical properties of the structural materials and superconducting coils are detailed in [22]. The nonlinear thermal contraction of the superconducting coils, which accounts for temperature dependence, is also derived from [22]. Sliding and separation contact elements are defined between the mandrels and both the superconducting and ESC coils, assuming a friction coefficient of 0.1. For the LTS coils in layers 5 and 6, the degrees of freedom of the nodes are coupled to the wedges, while separation from the poles is allowed. The model assumes no thermal propagation to the surrounding structure.

The stresses on the HTS and LTS superconducting coils are verified against the Von Mises equivalent stress criterion. To prevent conductor degradation, the allowable Von Mises stress is limited to 180 MPa for Nb_3Sn and 120 MPa for Bi-2212 [23], [24].

B. ESC transient simulation

The simulated currents during an ESC transient is shown in Fig. 3. The time required for quench detection, validation and triggering is assumed to be $t = 16$ ms. After triggering the ESC units, a positive current change is imposed in the ESC coils, with peak currents reaching approximately 1.8 kA for ESC 1 and 2.3 kA for ESC 2 and 3. Simultaneously, a negative current change is imposed in the superconducting coils. During this phase, the rapid current variation induces a large change in the total magnetic field, dB_{tot}/dt, within the magnet windings, which generates high inter-filament coupling loss in the superconductor, with a peak value of about 140 W/cm^3. As a result, nearly 100% of the LTS turns are quenched within 5–10 ms.

For a hybrid dipole magnet made of both HTS and LTS conductors, the adopted protection strategy is to deposit the stored energy primarily in the LTS windings that are easier to transfer to the normal-conducting state. Transient losses are also generated in the HTS coils; however, their local temperature at the end of the transient remains below 40 K.

Between 50 ms and 300 ms, the magnet is discharging, with both the magnet current and the ESC coil currents decreasing, while the temperature rises and all coils continue to heat up. During the final phase of the quench transient, lasting from 300 ms to 1000 ms, the currents in the magnet and ESC coils continue to decrease until completely discharged, while all coils keep heating up until the peak temperature is reached.

The temperature T (K) evolution in the windings of the HTS and LTS magnet coils is shown in Fig. 4. The 25/75 percentile is highlighted in a darker color for reference. The maximum temperature reached during the entire transient is below 240 K. Under adiabatic assumptions, i.e., neglecting heat diffusion to adjacent turns, the calculated hot-spot temperature is approximately 280 K, which is a level deemed safe with respect to permanent degradation [25].

The simulated voltages to ground developed in the magnet windings are shown in Fig. 5. The initial voltage peak,

This article has been accepted for publication in IEEE Transactions on Applied Superconductivity. This is the author's version which has not been fully edited and content may change prior to final publication. Citation information: DOI 10.1109/TASC.2026.3666509

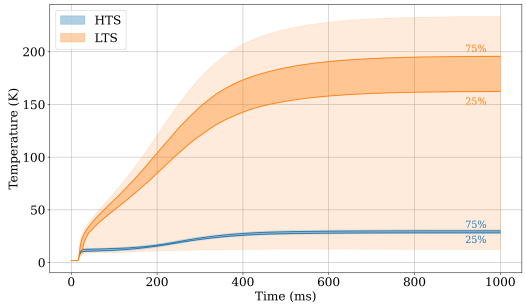

Fig. 4. Evolution of the temperature in the magnet coils as a function of time during a quench transient. The 25/75 percentile of both HTS and LTS coils is also added for reference.

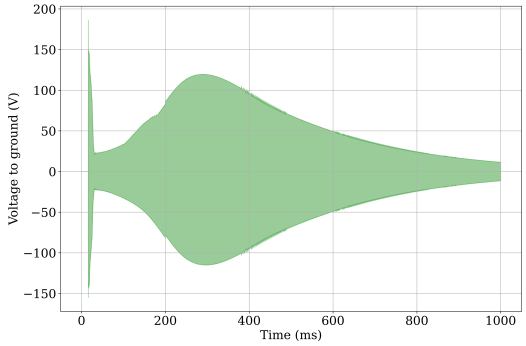

Fig. 5. Evolution of the voltages to ground of the magnet turns during a quench transient as a function of time.

observed within the first few milliseconds, is induced by the ESC coils, whereas the peak around 300 ms results from the sequence of inductive magnet coil sections and resistive ESC coil sections. The ESC-induced voltages and those resulting from the sequence of inductive and resistive voltage drops across the turns can cause the voltage to ground to reach positive and negative values. During the entire transient, the peak voltage to ground remains lower than 200 V, and the peak turn-to-turn voltage is lower than 8 V.

C. Mechanical transient

The evolution of the Von Mises equivalent stress in both the superconducting and copper ESC coils is shown in Fig. 6. The stress limits considered in the analysis are also plotted with dashed lines for comparison.

The thermo-mechanical transient associated with an ESC discharge following a quench is initiated at $t = 0$ ms. For $t \leq 0$, there is no current in the ESC coils and the magnet is powered at the nominal operating current I_{op}.

During the first 50 ms, the stresses in the magnet coils decrease as the magnet current is reduced, while the peak stresses in the ESC coils show a slight increase due to the rising current in these coils. The increase of the stresses in ESC coils is strongly influenced by the selected ESC unit parameters, namely their capacitance and charging voltage. Between 50 and 300 ms, the currents in both the magnet and the ESC coils decrease, while temperatures rise and all coils heat up. Electromagnetic-force-induced stresses decrease

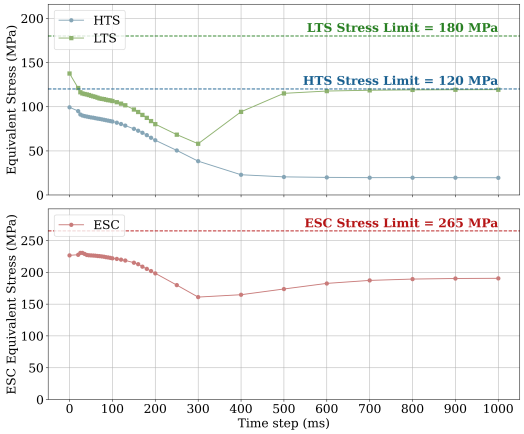

Fig. 6. Peak equivalent stress in the magnet (upper plot) and ESC (lower plot) coils during the transient initiated by triggering the ESC system at $t = 16$ ms. In the first 50 ms, stress in the ESC coils rises due to increasing current; from 50 to 300 ms, electromagnetic stresses decrease faster than thermal stresses increase, and from 300 to 1000 ms, thermal stresses dominate. The dashed lines indicate the maximum allowable stress values.

faster than thermal stresses increase. As a result, the stresses in the superconducting coils decrease during this phase.

Between 300 and 1000 ms, the currents in both the magnet and the ESC coils decrease to zero, while the stresses increase because the thermal stresses caused by the rising temperature grow faster than the reduction in electromagnetic-force-induced stresses. In this final phase, the stresses in the ESC coils do not depend on the ESC unit parameters, as they result from the energy transferred from the magnet coils to the ESC coils. The behavior of HTS coils differs from that of LTS coils during this phase. In HTS coils, the stresses continue to decrease as the coil temperature remains below 40 K, as shown in Fig. 4. In contrast, in LTS coils, the stresses initially decrease but rise again during the final phase due to the increasing temperature and the resulting thermal stresses.

The contour plots of the equivalent stress in the magnet and ESC coils are presented in Fig. 7. The results are presented as element contours on a mesh with a size of 1 mm to account for the insulation thickness. For both HTS and LTS coils, the stresses remain within acceptable limits during the entire quench transient. The peak stress occurs during magnet energization, as shown in Fig. 7(a), reaching 99 MPa for HTS coils and 138 MPa for LTS coils.

ESC coils in layers A and B experience higher stress levels than ESC coil in layer C. The peak stress in the ESC coils occurs at $t = 50$ ms, as shown in Fig. 7(b), and reaches 231 MPa. During the transient, a general decrease in stress is observed, as the reduction in current mitigates the effects of the electromagnetic forces. However, the temperature in the ESC coils continues to rise, leading to a subsequent increase in stress due to thermal expansion.

IV. Parametric Investigation

A parametric study is performed between STEAM-LEDET and ANSYS APDL to assess the influence of various design and operating parameters on the protection system performance. The parameters investigated include the ESC con-

This article has been accepted for publication in IEEE Transactions on Applied Superconductivity. This is the author's version which has not been fully edited and content may change prior to final publication. Citation information: DOI 10.1109/TASC.2026.3666509

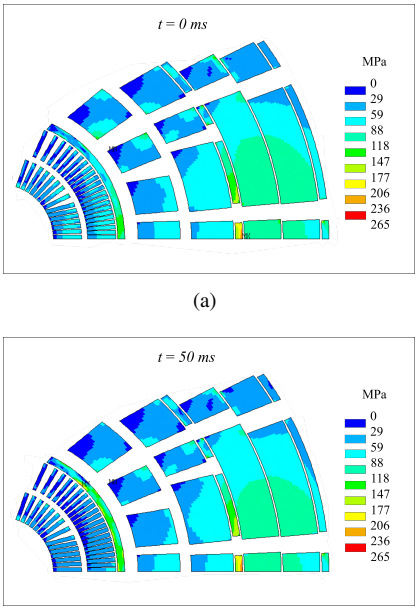

Fig. 7. Von Mises equivalent stress (MPa) in both superconductive and ESC coils during energization (a) and at t = 50 ms (b).

ductor size, ESC coil location, ESC unit voltage, and ESC conductor RRR. The objective is to identify a configuration capable of limiting both the adiabatic hot-spot temperature T_{hot} and the peak equivalent stresses. The post-processing analysis is focused on these two quantities, which served as key performance indicators for determining the feasibility and effectiveness of each design. The peak stresses in the superconducting coils are not addressed in this section, as they do not significantly affect the performance evaluation during quench transients.

As discussed in Section II-B, the copper selection for the ESC coils is based on electrical conductivity and mechanical strength at cryogenic temperatures. Based on the data presented in Fig. 2, the ratio between the simulated maximum equivalent stress in the ESC coils and the tensile yield strength of oxygen-free copper is evaluated. The results for the assessed designs, considering the various parameters involved, are shown in Fig. 8. In this plot, the x-axis represents the ratio between the adiabatic hot-spot temperature T_{hot} obtained from each simulation and the maximum allowed temperature, set at 300 K, while the y-axis represents the ratio between the maximum equivalent stress in the ESC coils and the tensile yield strength. Each marker corresponds to a specific ESC unit voltage configuration, and each color indicates the selected RRR value for each simulation. For instance, the green square represents a simulation in which the ESC unit voltage is 500 V for both ESC 1 and ESC 2-3 units and the RRR value is 100. The shaded region in the plot identifies the feasible designs, defined as those with both the stress ratio and the temperature ratio below unity. The reference simulation, whose results are presented in Section III, is identified by the pink cross and highlighted in the plot with a black circle.

The results indicate that, to ensure sufficient yield strength

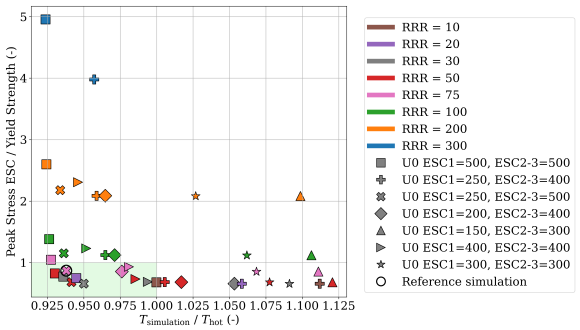

Fig. 8. Results of the parametric investigation. The x-axis shows the ratio between the simulated adiabatic hot-spot temperature and the maximum allowable value, while the y-axis shows the ratio between the simulated peak stress in the ESC coils and the tensile yield strength. Markers indicate ESC unit voltage configurations, and colors represent the selected RRR values. The shaded region denotes feasible designs, and the reference simulation is identified with the pink cross and highlighted with a black circle.

to meet the mechanical requirements without compromising electrical conductivity, a cold work percentage between 30% and 50% should be considered. The selected range ensures reliable performance within defined limits, with a sufficiently higher RRR between 50 and 75. Given the limited data on copper in wire form, a broader range of working possibilities is provided, although minimizing the cold work percentage is generally recommended to avoid potential manufacturability challenges.

V. Conclusion

In this contribution, a quench transient analysis is presented for a 20 T hybrid Bi-2212/Nb_3Sn cosθ dipole magnet integrated with Energy Shift with Coupling (ESC) protection system. The study combines two-dimensional electromagnetic-thermal simulations performed in STEAM-LEDET with two-dimensional mechanical analyses carried out in ANSYS APDL. In the simulations, a short-model version of the dipole with a magnetic length of 1 m is analyzed.

The parametric investigation shows that design configurations can be identified which satisfy the requirements for both the Von Mises equivalent stress and the adiabatic hot-spot temperature. The Von Mises equivalent stress remains within the specified allowable limits for all coils during the entire quench transient: 99 MPa for HTS, 138 MPa for LTS, and 231 MPa for ESC coils. The adiabatic hot-spot temperature is around 280 K, below the maximum allowable value of 300 K.

The proposed quench protection system design consists of ESC 1 powered by one 50 mF, 250 V unit, ESC 2 powered by one 50 mF, 500 V unit and ESC 3 powered by one 50 mF, 500 V unit. A cold work percentage of 30% is chosen as a suitable compromise between maintaining high electrical conductivity and meeting the mechanical strength requirements.

This study suggests the feasibility and effectiveness of an innovative quench protection system for high-field magnets, and demonstrates that thermo-mechanical stress evaluation, even when carried out through two-dimensional analysis, is essential during the quench transient for identifying design configurations that fully comply with all operational requirements.

REFERENCES

[1] P. Ferracin, G. Ambrosio, D. Arbelaez, L. Brouwer, E. Barzi, L. Cooley, L. G. Fajardo, R. Gupta, M. Juchno, V. Kashikhin, V. Marinozzi, I. Novitski, E. Rochepault, J. Stern, A. Zlobin, and N. Zucchi, "Towards 20 T hybrid accelerator dipole magnets," *IEEE Transactions on Applied Superconductivity*, vol. 32, 2022.

[2] P. Ferracin, G. Ambrosio, M. Anerella, D. Arbelaez, L. Brouwer, E. Barzi, L. D. Cooley, J. Cozzolino, L. Garcia Fajardo, R. Gupta, M. Juchno, V. V. Kashikhin, F. Kurian, V. Marinozzi, I. Novitski, E. Rochepault, J. Stern, G. Vallone, B. Yahia, and A. Zlobin, "Conceptual design of 20 T hybrid accelerator dipole magnets," *IEEE Transactions on Applied Superconductivity*, vol. 33, no. 5, pp. 1–7, 2023.

[3] L. Cooley, P. Ferracin, S. Gourlay, D. Larbalestier, M. Palmer, S. Prestemon, G. Velev, G. Ambrosio, D. Arbelaez, K. Badgley, L. Brouwer, D. Davis, J. L. Fernandez, V. Kashikhin, S. Krave, M. Marchevsky, I. Novitski, I. Pong, T. Shen, S. Stoynev, R. Teyber, G. Vallone, X. Wang, and X. Xu, "The 2025 roadmaps for the US Magnet Development Program," 2025. [Online]. Available: https://arxiv.org/abs/2508.19220

[4] E. Todesco, "Status and perspectives of high field magnets for particle accelerators," *IEEE Transactions on Applied Superconductivity*, vol. 35, no. 5, pp. 1–14, 2025.

[5] J. Ferradas Troitino, H. Bajas, L. Bianchi, B. Castaldo, P. Ferracin, M. Guinchard, S. Izquierdo, J. V. Lorenzo, F. Mangiarotti, J. C. Perez, E. Takala, G. Vallone, and C. Senatore, "A methodology for the analysis of the three-dimensional mechanical behavior of a Nb_3Sn superconducting accelerator magnet during a quench," *Superconductor Science and Technology*, vol. 34, no. 8, p. 084003, 2021. [Online]. Available: https://doi.org/10.1088/1361-6668/ac0952

[6] G. Vallone, E. Ravaioli, E. Anderssen, D. Arbelaez, J. R. Fernandez, and G. Sabbi, "Simulation of thermo-mechanical stresses after a quench in the 15 T Test Facility Dipole magnet," *IEEE Transactions on Applied Superconductivity*, vol. 34, no. 5, pp. 1–6, 2024.

[7] E. Ravaioli, V. I. Datskov, C. Giloux, G. Kirby, H. H. J. ten Kate, and A. P. Verweij, "New, coupling loss induced, quench protection system for superconducting accelerator magnets," *IEEE Transactions on Applied Superconductivity*, vol. 24, no. 3, pp. 1–5, 2014.

[8] E. Ravaioli, "CLIQ. A new quench protection technology for superconducting magnets," PhD Thesis - Research UT, graduation UT, University of Twente, Netherlands, 2015.

[9] E. Ravaioli, G. Ambrosio, D. Araujo, M. D'Addazio, P. Ferracin, R. Gupta, V. Marinozzi, E. Rochepault, G. Vallone, A. Verweij, M. Wozniak, and A. Zlobin, "Quench protection analysis of 20 T hybrid accelerator dipole magnets," *IEEE Transactions on Applied Superconductivity*, vol. 35, no. 5, pp. 1–5, 2025.

[10] E. Ravaioli, A. Verweij, and M. Wozniak, "Energy shift with coupling (ESC): a new quench protection method," *Superconductor Science and Technology*, vol. 38, no. 3, p. 035009, 2025. [Online]. Available: https://doi.org/10.1088/1361-6668/ada833

[11] E. Ravaioli, J. Bauche, M. Dumas, I. G.-A. Sanchez, F. Mangiarotti, M. Masci, J. C. Perez, A. Verweij, G. Willering, and M. Wozniak, "First experimental demonstration of the ESC protection method," *Superconductor Science and Technology*, vol. 38, no. 12, p. 125006, 2025. [Online]. Available: https://doi.org/10.1088/1361-6668/ae1894

[12] M. D'Addazio, P. Ferracin, V. Marinozzi, E. Ravaioli, G. Vallone, and L. Savoldi, "Conceptual structural design and analysis of a 20 T hybrid cos dipole for future particle colliders," *IEEE Transactions on Applied Superconductivity*, vol. 35, no. 5, pp. 1–5, 2025.

[13] V. Marinozzi, P. Ferracin, and G. Vallone, "Conceptual design of a 20 T hybrid cos-theta dipole superconducting magnet for future high-energy particle accelerators," *IEEE Transactions on Applied Superconductivity*, vol. 33, no. 5, pp. 1–5, 2023.

[14] G. H. Morgan, "Theoretical behavior of twisted multicore superconducting wire in a time-varying uniform magnetic field," *Journal of Applied Physics*, vol. 41, no. 9, pp. 3673–3679, 1970. [Online]. Available: https://doi.org/10.1063/1.1659491

[15] J. Carr, W. J., "AC loss in a twisted filamentary superconducting wire," *Journal of Applied Physics*, vol. 45, no. 2, pp. 935–938, 1974. [Online]. Available: https://doi.org/10.1063/1.1663342

[16] A. P. Verweij, "Electrodynamics of superconducting cables in accelerator magnets," Ph.D. dissertation, Twente U., 1995.

[17] E. Ravaioli, B. Auchmann, G. Chlachidze, M. Maciejewski, G. Sabbi, S. E. Stoynev, and A. Verweij, "Modeling of interfilament coupling currents and their effect on magnet quench protection," *IEEE Transactions on Applied Superconductivity*, vol. 27, no. 4, pp. 1–8, 2017.

[18] N. J. Simon, E. S. Drexler, and R. P. Reed, "Properties of copper and copper alloys at cryogenic temperatures," National Inst. of Standards and Technology (MSEL), Boulder, CO (United States). Materials Reliability Div., Tech. Rep., 1992. [Online]. Available: https://www.osti.gov/biblio/5340308

[19] G. Kirby, V. Datskov, S. Clement, A. Chiuchiolo, P. Fessia, R. Gauthier, G. Lynch, J. Murtomaki, J. van Nugteren, F. Pincot, J. C. Perez, L. Rossi, G. De Rijk, and S. Tavares, "Thermal contraction, experimental data and fits for the thermal contraction of future magnet materials at cryogenic temperatures," CERN, 2016.

[20] E. Ravaioli, B. Auchmann, M. Maciejewski, H. ten Kate, and A. Verweij, "Lumped-Element Dynamic Electro-Thermal model of a superconducting magnet," *Cryogenics*, vol. 80, pp. 346–356, 2016, chats on Applied Superconductivity 2015 University of Bologna, Italy, 14-16 September 2015. [Online]. Available: https://www.sciencedirect.com/science/article/pii/S0011227516300832

[21] "STEAM: Simulation of Transient Effects in Accelerator Magnets," CERN. [Online]. Available: https://cern.ch/steam

[22] G. Vallone, E. Anderssen, B. Bordini, and P. Ferracin, "A review of the mechanical properties of materials used in Nb_3Sn magnets for particle accelerators," *IEEE Transactions on Applied Superconductivity*, vol. 33, no. 5, pp. 1–6, 2023.

[23] H. Felice, M. Bajko, B. Bingham, B. Bordini, L. Bottura, S. Caspi, G. De Rijk, D. Dietderich, P. Ferracin, C. Giloux, A. Godeke, R. Hafalia, A. Milanese, L. Rossi, and G. L. Sabbi, "Performance of a Nb_3Sn quadrupole under high stress," *IEEE Transactions on Applied Superconductivity*, vol. 21, no. 3, pp. 1849–1853, 2011.

[24] S. Otten *et al.*, "Transverse stress test of two Bi-2212 Rutherford cables," presented at the General MDP Meeting, Zoom Webinar, July 19, 2023. [Online]. Available: https://conferences.lbl.gov/event/1402/

[25] G. Ambrosio, "Maximum allowable temperature during quench in Nb_3Sn accelerator magnets," 2014. [Online]. Available: http://cds.cern.ch/record/1643437